Letter

Pair production in circularly polarized waves

Christian Kohlfürst*

Helmholtz-Zentrum Dresden-Rossendorf, Bautzner Landstraße 400, 01328 Dresden, Germany

(Received 1 February 2023; accepted 2 December 2024; published 30 December 2024)

We study electron-positron pair production within two counterpropagating, circularly polarized electromagnetic fields through the Wigner formalism. We numerically generate high-resolution momentum maps to perform a detailed spectroscopic analysis. We identify signatures of polarization and kinematics of the incident fields in the final positron distribution and, on this basis, provide an intuitive picture of helicity transfer in multiphoton pair production.

DOI: 10.1103/PhysRevD.110.L111903

Introduction. Quantum Electrodynamics (QED) might be the most accurate and most precisely tested theory of physics. However, despite all its success, technological limitations have left large sectors of the theory almost completely unexplored [1–3].

It was only at the turn of the millennium that first observations in nonlinear QED were made in collisions of electron beams with laser light [4,5]. These experiments proved to be a milestone in the development of strong-field QED, sparking renewed interest in laser-matter interactions at the extreme, cf. Ref. [6]. In the following years, further progress in technology has led to the funding of new, ultrahigh-intensity laser facilities [7], particle accelerators that are capable of probing purely electromagnetic interactions in ultraperipheral collisions [8], and breakthroughs in the production of high-energy electron and photon beams [9–11]. Because of these advancements, it is thus finally possible to explore the strong-field aspects of QED putting to a test our understanding of nonequilibrium physics [12] and fundamental particle physics [13,14], as well as emergent phenomena [15,16].

In this Letter our focus is on multiphoton pair production [17], in particular, the transfer of energy, helicity, and momentum from photons to the newly created electrons and positrons, a topic that is also of interest in atomic physics, as the photon momentum transfer in the ionization of hydrogen (or positronium [22] for that matter [23]) functions similarly [24,25]. Furthermore, studying pair production is expected to generate further insight into photoelectron momentum transfer in stellar objects [26], laser-plasma interactions [27,28], quantum optics [29], and helicity transfer in electron-photon systems [30,31].

To this end, we discuss nonperturbative pair production in high-frequency, circularly polarized fields through employing the Wigner formalism, i.e., relativistic quantum kinetic theory [32–34]. Within this approach, quantum statistical as well as further collective strong-field QED effects are already included, e.g., a field-dependent shift in the particles' effective mass [35]. We take into account dependencies on $\hbar$ nonperturbatively, not relying on any form of gradient expansion. On the contrary, within our formalism we explicitly go beyond any dipole or even locally constant field approximation [36]. The particle momentum spectra, in particular, photopositron angular distributions, are analyzed with respect to the waves' handedness and the transfer of helicity from the photon field to the particle pair [37–39]. We relate the outcome of our simulations to predictions from a simple semiclassical model in order to gain a more intuitive picture of the underlying physical processes [40,41].

We use natural units ($\hbar = c = 1$) throughout and display results in terms of electron mass $m = 511$ keV and critical field strength $E_{\mathrm{cr}} = m^2/e \approx 1.3 \times 10^{18}$ V/m. Furthermore, Supplemental Material is provided that contains additional theoretical background and discusses technical aspects in greater detail [42].

Theoretical formalism. We discuss nonperturbative particle production as a many-body problem with an initial vacuum state being exposed to, and therefore driven out of equilibrium, by an external electromagnetic field [60,61].

The time evolution of fermions coupled to a gauge field, e.g., an electromagnetic field in the mean-field or Hartree approximation is given by the Dirac equation

$$\left(\mathrm{i}(\partial_\mu + \mathrm{i}eA_\mu(x))\gamma^\mu - m\right)\hat{\Psi}(x) = 0, \tag{1}$$

*Contact author: c.kohlfuerst@hzdr.de

Published by the American Physical Society under the terms of the Creative Commons Attribution 4.0 International license. Further distribution of this work must maintain attribution to the author(s) and the published article's title, journal citation, and DOI. Funded by SCOAP³.

where the spinor $\hat{\Psi}(x)$ is quantized, but the vector potential $A_\mu(x)$ is treated as a background field and not as a dynamical operator.

We are, in particular, interested in particle-antiparticle correlations of the form $\langle\hat{\bar{\Psi}}(x)\hat{\Psi}(y)\rangle$ in the pairs' phase space as they can be interpreted in terms of particle distribution functions [62,63]. To this end, a Fourier transform from relative coordinate $\mathfrak{s} = y - x$ to kinetic momentum p is performed while the center-of-mass coordinate $r = (x + y)/2$ is maintained [64].

Considering that the corresponding correlation functions must obey gauge invariance, the covariant Wigner operator is introduced as follows [65,66]:

$$\hat{\mathcal{W}}(r,p) = \frac{1}{2}\int \mathrm{d}^4\mathfrak{s}\, \mathrm{e}^{\mathrm{i}p_\mu\mathfrak{s}^\mu}\, \mathrm{e}^{\mathrm{i}e\int_{-1/2}^{1/2}\mathrm{d}\xi\,\mathfrak{s}^\mu A_\mu(r+\xi\mathfrak{s})} \times\left[\hat{\bar{\Psi}}(r-\mathfrak{s}/2),\hat{\Psi}(r+\mathfrak{s}/2)\right]. \tag{2}$$

On this basis, we derive quantum kinetic equations that describe the interaction of polarized, correlated fermions with strong electromagnetic background fields. Hereby, the Dirac equation (1) for the vacuum expectation value of the Wigner operator $\mathbb{W}(r,p) = \langle\hat{\mathcal{W}}(r,p)\rangle$ reads

$$\left[\left(\Pi_\mu + \frac{\mathrm{i}}{2}D^r_\mu\right)\gamma^\mu - m\right]\mathbb{W}(r,p) = 0, \tag{3}$$

with momentum and derivative operator being augmented by the field-strength tensor $F_{\mu\nu} = \partial_\mu A_\nu - \partial_\nu A_\mu$,

$$D^r_\mu = \partial^r_\mu - e\int_{-1/2}^{1/2}\mathrm{d}\xi\, F_{\mu\nu}(r - \mathrm{i}\xi\partial_p)\partial_p^\nu, \tag{4}$$

$$\Pi_\mu = p_\mu - \mathrm{i}e\int_{-1/2}^{1/2}\mathrm{d}\xi\,\xi F_{\mu\nu}(r - \mathrm{i}\xi\partial_p)\partial_p^\nu. \tag{5}$$

Ultimately, after expanding the matrix-valued Wigner function $\mathbb{W}(r,p)$ into Dirac bilinears and projection on equal time

$$\mathbb{w}(t,\boldsymbol{x},\boldsymbol{p}) = \int\frac{\mathrm{d}p_0}{2\pi}\mathbb{W}(r,p), \tag{6}$$

where $r = (t,\boldsymbol{x})$, we obtain the quantum transport equations in terms of, e.g., mass $\mathbb{s}$, charge $\mathbb{v}_0$, and current density $\mathbb{v}$ [67],

$$D_t\mathbb{s} - 2\boldsymbol{\Pi}\cdot\mathbb{t}_{\mathbb{1}} = 0, \tag{7}$$

$$D_t\mathbb{p} + 2\boldsymbol{\Pi}\cdot\mathbb{t}_{\mathbb{2}} = -2m\mathbb{a}_0, \tag{8}$$

$$D_t\mathbb{v}_0 + \boldsymbol{D}\cdot\mathbb{v} = 0, \tag{9}$$

$$D_t\mathbb{a}_0 + \boldsymbol{D}\cdot\mathbb{a} = +2m\mathbb{p}, \tag{10}$$

$$D_t\mathbb{v} + \boldsymbol{D}\mathbb{v}_0 + 2\boldsymbol{\Pi}\times\mathbb{a} = -2m\mathbb{t}_{\mathbb{1}}, \tag{11}$$

$$D_t\mathbb{a} + \boldsymbol{D}\mathbb{a}_0 + 2\boldsymbol{\Pi}\times\mathbb{v} = 0, \tag{12}$$

$$D_t\mathbb{t}_{\mathbb{1}} + \boldsymbol{D}\times\mathbb{t}_{\mathbb{2}} + 2\boldsymbol{\Pi}\mathbb{s} = +2m\mathbb{v}, \tag{13}$$

$$D_t\mathbb{t}_{\mathbb{2}} - \boldsymbol{D}\times\mathbb{t}_{\mathbb{1}} - 2\boldsymbol{\Pi}\mathbb{p} = 0, \tag{14}$$

and equal-time derivative operators [68,69]

$$D_t = \partial_t + e\int_{-1/2}^{1/2}\mathrm{d}\xi\,\boldsymbol{E}(\boldsymbol{x} + \mathrm{i}\xi\boldsymbol{\nabla}_p, t)\cdot\boldsymbol{\nabla}_p, \tag{15}$$

$$\boldsymbol{D} = \boldsymbol{\nabla}_x + e\int_{-1/2}^{1/2}\mathrm{d}\xi\,\boldsymbol{B}(\boldsymbol{x} + \mathrm{i}\xi\boldsymbol{\nabla}_p, t)\times\boldsymbol{\nabla}_p, \tag{16}$$

$$\boldsymbol{\Pi} = \boldsymbol{p} - \mathrm{i}e\int_{-1/2}^{1/2}\mathrm{d}\xi\,\xi\boldsymbol{B}(\boldsymbol{x} + \mathrm{i}\xi\boldsymbol{\nabla}_p, t)\times\boldsymbol{\nabla}_p. \tag{17}$$

This set of equations is closed, a consequence of the mean-field approximation for external fields in which the Bogoliubov-Born-Green-Kirkwood-Yvon hierarchy truncates at the one-body level [68]. The asymptotic particle n and charge density q is determined once the electromagnetic pulse has had sufficient time to slowly fade away, cf. Refs. [70–72] for discussions on expectation values at intermediate times,

$$n(z,\boldsymbol{p}) = \frac{m(\mathbb{s} - \mathbb{s}_{\mathrm{vac}}) + \boldsymbol{p}\cdot(\mathbb{v} - \mathbb{v}_{\mathrm{vac}})}{2\sqrt{m^2 + \boldsymbol{p}^2}}, \tag{18}$$

$$q(z,\boldsymbol{p}) = \mathbb{v}_0. \tag{19}$$

We use vacuum initial conditions, so only the mass and charge densities are initially nonzero,

$$\mathbb{s}_{\mathrm{vac}}(\boldsymbol{p}) = -\frac{2m}{\sqrt{m^2+\boldsymbol{p}^2}}, \quad \mathbb{v}_{\mathrm{vac}}(\boldsymbol{p}) = -\frac{2\boldsymbol{p}}{\sqrt{m^2+\boldsymbol{p}^2}}. \tag{20}$$

Integrations over spatial coordinates in phase space yield the mean particle distribution $f(\boldsymbol{p})$. Further integrating also over momentum coordinates gives the mean particle number. In consequence, this formalism constitutes the generalization of the classical Vlasov equation as well as the Bargmann-Michel-Telegdi equations to the relativistic quantum domain.

Model for the fields. External fields are modeled after polarized plane waves propagating in the z direction,

$$A_0 = 0, \qquad \mathbf{A}(t,z) = f(t)\begin{pmatrix}\varepsilon/\omega\cos(\omega t + kz)\\ \varepsilon\sigma/\omega\sin(\omega t + kz)\\ 0\end{pmatrix}, \tag{21}$$

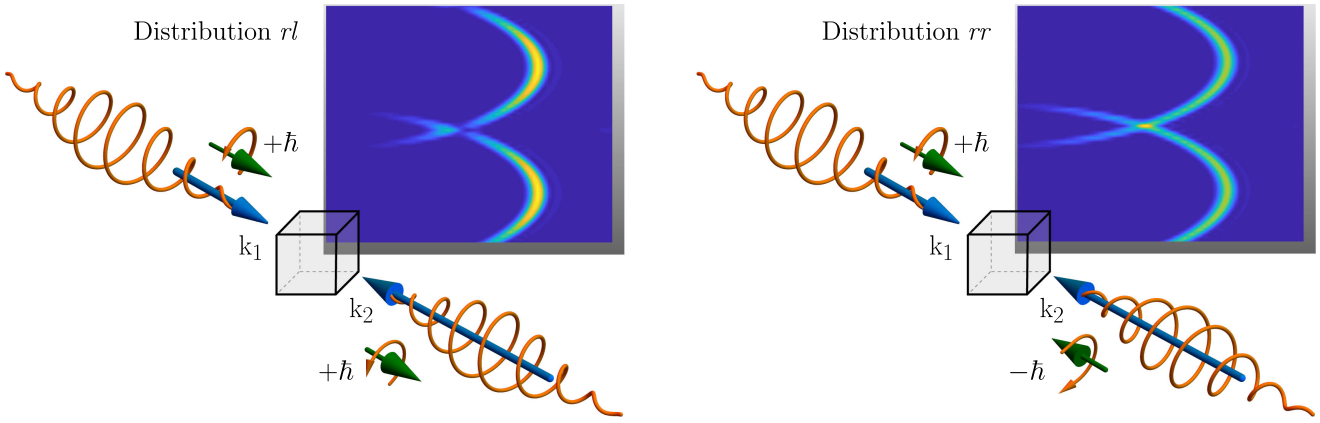


FIG. 1. Sketch of the two scenarios; *rl* or "right-handed, left-handed" on the left and *rr* or "right-handed, right-handed" on the right. Two circularly polarized fields with wave vectors $\mathrm{k}_1 = (\omega_1, 0, 0, k_1)$ and $\mathrm{k}_2 = (\omega_2, 0, 0, k_2)$, respectively, collide within an interaction region represented here by a box. Electron-positron pairs that exceed the threshold for particle production are evaluated in terms of distribution functions. The differences in polarization of the incident waves $\pm\hbar$ manifests itself in characteristic signatures in the particles' momentum distribution.

where $f(t)$ is introduced as an overall damping term such that $\mathbf{A}(t, z)$ vanishes at asymptotic times. Periodicity confines the spatial dimension to a length $2\pi/|k|$. Physical parameters are the peak field strength ε, the field frequency $\omega = |k|$, and the quantity $\sigma = \pm 1$ which controls the handedness of the waves.

A single external field of the form of Eq. (21) is incapable of creating particles as both Lorentz invariants, $\mathbf{E}^2 - \mathbf{B}^2$ and $\mathbf{E} \cdot \mathbf{B}$, vanish. To maximize the yield, we therefore resort to configurations with two counterpropagating fields (unlike atomic ionization where often copropagating fields are used [73]). Hereby, the strength and frequency of each wave are chosen independently, while we consider only two configurations with respect to the fields' handedness: in the *rl* scenario we have one right-handed and one left-handed wave, whereas the *rr* scenario features two right-handed fields, cf. Fig. 1.

Note that the photons constituting the fields (21) carry energy and momentum, as well as helicity. In this regard, the proposed setup, in particular, the *rr* scenario, is much more advanced than comparable models that employ either a local or rotating dipole approximation, where pair production is evaluated at $z = 0$ only [74–78].

On a further note, with fields of the form of Eq. (21) the fields embedded in the operators D_l, $\boldsymbol{D}$, and $\boldsymbol{\Pi}$ already indicate a discrete momentum transfer from photons to the electron-positron pair (see Supplemental Material [42]).

Absorption model. The Wigner formalism provides access to particle kinematics in unprecedented detail. In particular, it creates the possibility to study the particle phase space in its entirety. In this section, we complement the results obtained by numerical simulations with an auxiliary absorption model that further illuminates specific aspects of pair production and acts as a guideline toward building an intuitive understanding.

The basic idea is to view electron-positron pair production within external fields as an ionization of a bound state (similar to the ionization of hydrogen or positronium). The argument is as follows. The background field has to provide enough energy for the particle to be "ionized." Given that there are n photons that constitute a multiphoton absorption process, the total energy of these photons has to exceed the electron-positron rest mass, $2m \sim 1.022$ MeV, in order to overcome the ionization threshold. This simple relation is complicated by the fact that for high-frequency fields we have to respect the photon momentum transfer. Therefore, it is the four-vector energy-momentum conservation that has to hold [79–81].

Accordingly, it is the number of photons absorbed per wave, n_1 and n_2, rather than the total number n that provides the accurate characterization. Therefore, we have different channels contributing to the pair production process, which we distinguish by the different number of participating photons from each wave, e.g., $n_1 - n_2$.

In the dipole approximation, e.g., in laser-atom ionization, the momentum components are generally disregarded on the basis of different scales in the temporal and spatial domain. Only recently has the photon as a momentum carrier drawn interest also in nonrelativistic regimes [82].

The second important quantity is helicity for photons and angular momentum for fermions. Photons are massless spin-1 particles, thus each photon has a helicity of ± 1. The ratio of all photon helicities in a wave then constitutes the wave's polarization. In case of a circularly polarized wave, for example, all photons exhibit the same helicity. Because of angular momentum conservation in multiphoton pair production, this helicity is transferred to the electron-positron state, where it manifests in the form of spin S and orbital L angular momentum. In a state with antiparallel spin we have $S = 0$, while for a state with spins aligned we obtain $S = 1$; very similar to positronium [37,40]. It is assumed that LS coupling applies, in which case the total angular momentum

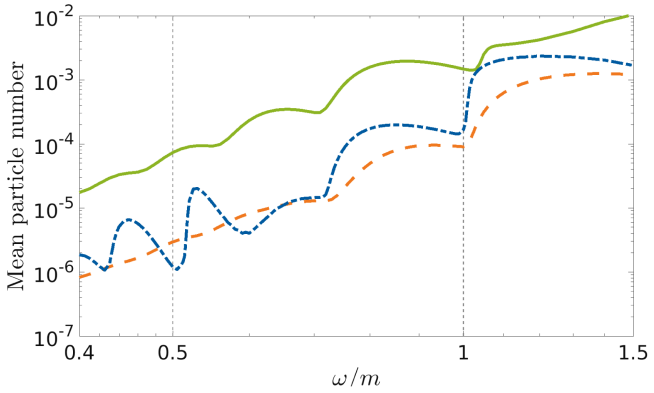


FIG. 2. Log-log plot of the mean particle number as a function of the fields' frequencies $\omega = \omega_1 = \omega_2$. The dashed orange line gives the number of created particles in the rl scenario. In contrast, the blue curve illustrates the result obtained for the rr scenario where both waves are right handed. The green curve serves as a means for comparison displaying the normalized yield in the rl scenario in a rotating dipole approximation, i.e., at the node of the standing wave where the magnetic field vanishes and the electric field is purely time dependent. Field strengths were fixed to $e\varepsilon_1 = e\varepsilon_2 = 0.1m^2$.

is then given by the vector sum $\mathbf{J} = \mathbf{L} + \mathbf{S}$. Therefore, any total helicity the incident photons provide (in our scenarios $n_1 \pm n_2$), that is not used to create the intrinsic spin of the electron-positron pair, has to show up in the orbital angular momentum [83,84].

Discussion. It is illuminating to first study the helicity sensitivity of the total particle yield [85,86], cf. Fig. 2. Here, we consider symmetric configurations with both waves having a field strength $e\varepsilon = 0.1m^2$ and frequency ω. In the rl scenario, helicity points in the direction of propagation for one wave and opposite that of the other. Thus, both waves supply the particle pair with a positive angular momentum (without restriction of generality), cf. Fig. 1. This scenario is also accessible through the rotating dipole approximation, where only energy and angular momentum transfer is considered. In this regard, the latter serves as point of contact to the broader literature. In the rr scenario, in principle, any integer number angular momentum can be probed.

Overall, the mean particle number in Fig. 2 for these two scenarios behaves similarly. There is an overall increase in the yield as a function of the field frequency, because the higher the individual photon energies, the more channels are "open" and, in turn, can contribute. The rotating dipole approximation overestimates the yield as it factors in unphysical channels, e.g., contributions from channels where either n_1 or n_2 is zero [87], and becomes unreliable close to the threshold $\sim 2m$ as it allows a single photon to decay.

There is a big difference in the strength of the signal around an n-photon resonance, though. This disparity is best analyzed in terms of the particles' momentum distribution. For example, at a frequency of $\omega = 0.5m$, thus close to the four-photon resonance, we observe the formation of particles at rest in the rr scenario, cf. Fig. 3(b), as particles are simply unable to amount a great surplus of kinetic energy. Such a situation is hindered, however, in an rl setup where, instead of a clear peak at the origin, the dominant contribution toward the yield comes from higher-order absorption channels, cf. Fig. 3(c). Upon closer inspection, Fig. 3(a), we find that the latter actually does not create any particles along the z axis.

By means of the absorption model, we interpret the situation as follows. The classical orbital angular momentum is given by $\boldsymbol{L} = \boldsymbol{r} \times \boldsymbol{p}$. If a particle moves straight in the

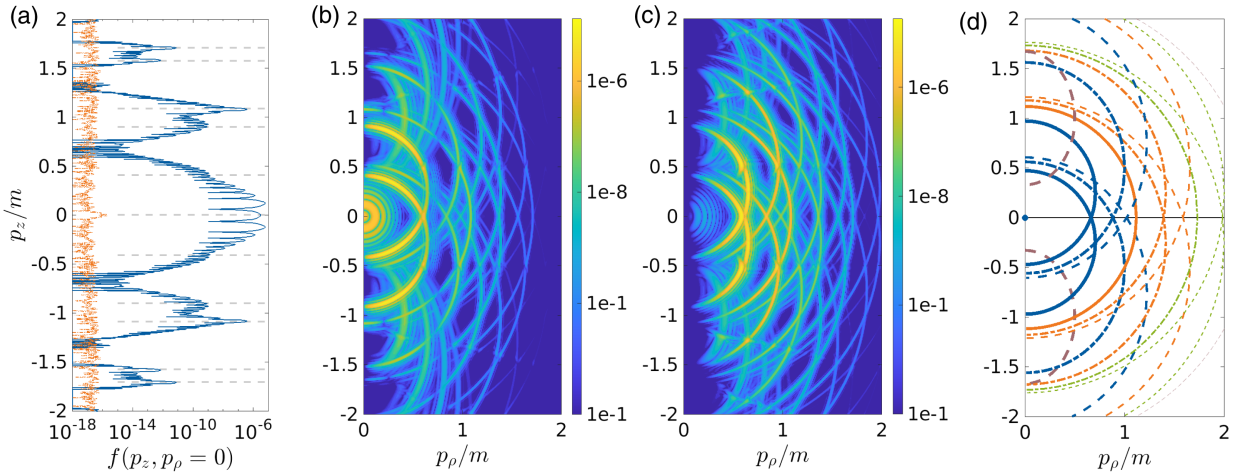


FIG. 3. (a) Particle distributions along p_z for the rl scenario (orange) and the rr scenario (blue) with indicators for the various nonvanishing channels (channels 2–2 at $p_z \approx 0$, 2–3 and 3–3 at $p_z \approx m$, as well as 3–4, 4–4 at $p_z \approx 1.6m$). Particle momentum maps in $p_\rho p_z$ for the rr scenario (b) as well as for the rl scenario (c) further highlight the substantial difference in particle bunching at small (transversal) momentum. (d) Sketch displaying various multiphoton channels to improve orientation in the momentum maps. Structure is as follows: blue indicates channels $n-2$, orange $n-3$, green $n-4$, and brown $n-5$ (includes mirrored counterparts). The brighter the color, the smaller the respective number of particles n. Field parameters: $\omega_1 = \omega_2 = 0.5m$ and $e\varepsilon_1 = e\varepsilon_2 = 0.1m^2$.

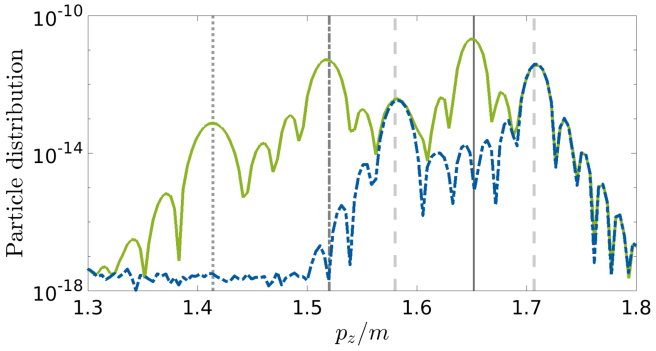


FIG. 4. Logarithmic plot of the particle distribution for the *rr* scenario at vanishing p_ρ (blue) and at $p_\rho = 0.015m$ (green). The gray lines indicate spectral peaks helping to distinguish them from quantum interferences. In the green curve the orbital angular momentum can be nonzero, opening up new channels, e.g., 4–2. Field parameters: $e\varepsilon_1 = e\varepsilon_2 = 0.1m^2$ and $\omega_1 = \omega_2 = 0.5m$.

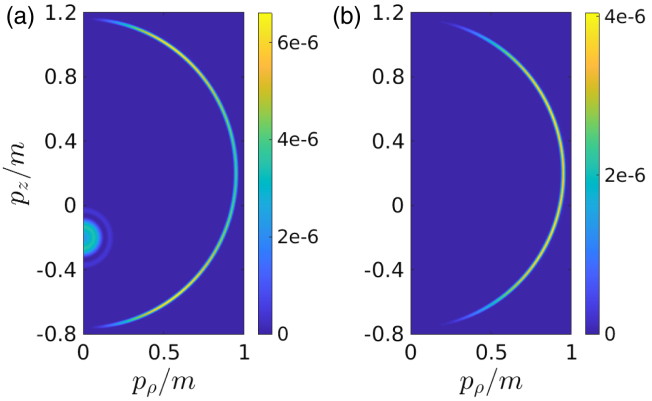


FIG. 5. Contour plot of positron distributions for the *rr* scenario (a) and the *rl* scenario (b) in a two-frequency setup (peak field strengths $e\varepsilon_1 = 0.01m^2$, $e\varepsilon_2 = 0.1m^2$, frequencies $\omega_1 = 1.2m$, $\omega_2 = 0.8m$). Positrons produced through the 1–2 channel (semicircle of radius m) exhibit a different angular profile depending on the scenario. Additionally, only in the *rr* scenario the 1–1 channel ($p_\rho \approx 0$, $p_z \approx -0.3m$) is contributing to the mean particle distribution.

z direction, the transversal momenta p_ρ are zero, thus the criterion for a particle ejection along p_z is that $\boldsymbol{L}$ has to vanish.

In the *rl* scenario, helicity is always positive, hence the total angular momentum of a pair is equal to the number of photons absorbed $J = n$. But as the intrinsic spin of the pair S is either zero or one, and due to the fact that energy-momentum conservation prevents a single photon from decaying, a pair's orbital angular momentum is thus always nonzero, $L = n - S > 0$. The necessary condition is therefore never satisfied. This situation is similar to a circularly polarized field interacting either with a quantized photon [38,88,89] or the field of a nucleus [90,91]. In both cases, the large total angular momentum impedes particle production. Contrariwise, in the *rr* scenario there are multiple opportunities to form a state with $L = 0$ as contributions to the angular momentum with opposite signs are indeed possible.

In the *rr* scenario, a complementary spectral analysis is performed for $p_\rho = 0.015m$, cf. Fig. 4. A comparison with Fig. 3(a) reveals that multiple new peaks appear, despite the fact that the transversal momentum only varies slightly. In such a case, however, the particles acquire a nonzero transversal momentum, which allows the orbital angular momentum to assume any value. Consequently, a greater number of channels are open, cf. Fig. 3(d).

Our approach is also applicable to pair creation through higher harmonics [92]. For two-frequency configurations the positron (or electron) distributions are asymmetric in p_z as $k_1 \neq k_2$. Specifically, in Fig. 5 we have $k_1 = 3k_0$, $k_2 = 2k_0$ with fundamental frequency $k_0 = 0.4m$. Consequently, particles created, e.g., through the 2–1 channel, acquire a much higher kinetic energy than particles created through the 1–2 channel.

In the *rl* scenario the angular momentum absorbed from the waves again stack, thus no positrons are created along p_z and, in turn, no traces of the 1–1 channel are to be found, cf. Fig. 5(b). For comparison, in the *rr* scenario the distribution function corresponding to the 1–2 channel peaks at a different emission angle of roughly 45° (and 135°) but does not vanish at $p_\rho = 0$ (at $p_z = 1.2m$ it has retained 1% of its maximal value). Additionally, two-photon pair production is entirely possible, cf. Fig. 5(a).

This apparent difference regarding the main emission angle might also be of interest with respect to modern searches for the Breit-Wheeler process [93–100]. Depending on the experimental setup, it might be preferential to actively search for an optimal beam polarization such that the particle emission is maximal for a specific angle.

Conclusion. In this Letter, we consider pair production through two counterpropagating, circularly polarized waves. We observe that the particles' orbital angular momentum and thus their emission direction is highly sensitive to the incident waves' polarization. Ejection along the photon propagation direction is completely blocked in interactions of a right-handed with a left-handed wave. Consequently, signatures of resonances in the particle yield are smoothed and shifted toward higher frequencies, i.e., particles have to acquire a higher kinetic energy. For two right-handed waves of similar frequency, no such restriction is found. This behavior extends to bifrequent fields as well.

Acknowledgments. We want to thank Ralf Schützhold and Naser Ahmadiniaz for the interesting discussions. We are particularly grateful for the assistance given by Nina Elkina regarding high-performance computing. Computations have been performed on the Hemera-Cluster in Dresden.

Data availability. The data that support the findings of this article are openly available [101].

[1] T. Heinzl and A. Ilderton, Eur. Phys. J. D **55**, 359 (2009).
[2] M. Marklund and J. Lundin, Eur. Phys. J. D **55**, 319 (2009).
[3] H. Gies, Eur. Phys. J. D **55**, 311 (2009).
[4] D. L. Burke, R. C. Field, G. Horton-Smith *et al.*, Phys. Rev. Lett. **79**, 1626 (1997).
[5] C. Bamber, S. J. Boege, T. Koffas *et al.*, Phys. Rev. D **60**, 092004 (1999).
[6] A. Fedotov, A. Ilderton, F. Karbstein, B. King, D. Seipt, H. Taya, and G. Torgrimsson, Phys. Rep. **1010**, 1 (2023).
[7] J. W. Yoon, Y. G. Kim, I. W. Choi, J. H. Sung, H. W. Lee, S. K. Lee, and C. H. Nam, Optica **8**, 630 (2021).
[8] J. Adam *et al.* (STAR Collaboration), Phys. Rev. Lett. **127**, 052302 (2021).
[9] V. Yakimenko, L. Alsberg, E. Bong *et al.*, Phys. Rev. Accel. Beams **22**, 101301 (2019).
[10] H. Abramowicz *et al.*, Eur. Phys. J. Special Topics **230**, 2445 (2021).
[11] A. Ringwald, Phys. Lett. B **510**, 107 (2001).
[12] D. Kremp, Th. Bornath, M. Bonitz, and M. Schlanges, Phys. Rev. E **60**, 4725 (1999).
[13] S. Meuren, C. H. Keitel, and A. Di Piazza, J. High Energy Phys. 06 (2015) 127.
[14] S. Evans and R. Schützhold, Phys. Rev. D **109**, L091901 (2024).
[15] K. Qu, S. Meuren, and N. J. Fisch, Phys. Rev. Lett. **127**, 095001 (2021).
[16] S. Meuren, D. A. Reis, R. Blandford *et al.*, arXiv: 2105.11607.
[17] For clarification, in the literature one distinguishes between different mechanisms of pair production [18–21]. Here, we consider particle creation through nonquantized "background" fields. Nevertheless, we still use the term "photon" as an electromagnetic wave can be considered a collection of energy packets with specific energy and momentum. In this context, the term "multiphoton pair production" refers to the interaction of coherent photons within such c-number fields.
[18] F. Sauter, Z. Phys. **69**, 742 (1931).
[19] J. S. Schwinger, Phys. Rev. **82**, 664 (1951).
[20] G. Breit and J. A. Wheeler, Phys. Rev. **46**, 1087 (1934).
[21] H. R. Reiss, J. Math. Phys. (N.Y.) **3**, 59 (1962).
[22] P. A. Zyla *et al.* (Particle Data Group), Prog. Theor. Exp. Phys. **2020**, 083C01 (2020).
[23] P. Moskal, A. Gajos, M. Mohammed *et al.*, Nat. Commun. **12**, 5658 (2021).
[24] C. T. L. Smeenk, L. Arissian, B. Zhou, A. Mysyrowicz, D. M. Villeneuve, A. Staudte, and P. B. Corkum, Phys. Rev. Lett. **106**, 193002 (2011).
[25] S. Chelkowski, A. D. Bandrauk, and P. B. Corkum, Phys. Rev. Lett. **113**, 263005 (2014).
[26] M. J. Seaton, J. Phys. B **28**, 3185 (1995).
[27] C. P. Ridgers, C. S. Brady, R. Duclous, J. G. Kirk, K. Bennett, T. D. Arber, A. P. L. Robinson, and A. R. Bell, Phys. Rev. Lett. **108**, 165006 (2012).
[28] D. Seipt and A. G. R. Thomas, Phys. Plasmas **30**, 093102 (2023).
[29] A. Gorlach, O. Neufeld, N. Rivera, O. Cohen, and I. Kaminer, Nat. Commun. **11**, 4598 (2020).
[30] F. L. Li, Y.-Y. Chen, K. Z. Hatsagortsyan, and C. H. Keitel, Phys. Rev. Lett. **128**, 174801 (2022).
[31] D. Seipt and B. King, Phys. Rev. A **102**, 052805 (2020).
[32] S. M. Schmidt, D. Blaschke, G. Ropke, S. A. Smolyansky, A. V. Prozorkevich, and V. D. Toneev, Int. J. Mod. Phys. E **07**, 709 (1998).
[33] Y. Kluger, J. M. Eisenberg, B. Svetitsky, F. Cooper, and E. Mottola, Phys. Rev. D **45**, 4659 (1992).
[34] R. Alkofer, M. B. Hecht, C. D. Roberts, S. M. Schmidt, and D. V. Vinnik, Phys. Rev. Lett. **87**, 193902 (2001).
[35] C. Harvey, T. Heinzl, A. Ilderton, and M. Marklund, Phys. Rev. Lett. **109**, 100402 (2012).
[36] A. Blinne and E. Strobel, Phys. Rev. D **93**, 025014 (2016).
[37] M. J. A. Jansen, J. Z. Kamiński, K. Krajewska, and C. Müller, Phys. Rev. D **94**, 013010 (2016).
[38] S. Villalba-Chavez and C. Muller, Phys. Lett. B **718**, 992 (2013).
[39] A. Golub, S. Villalba-Chávez, and C. Müller, Phys. Rev. D **103**, 096002 (2021).
[40] C. Kohlfürst, Phys. Rev. D **99**, 096017 (2019).
[41] I. A. Aleksandrov and A. Kudlis, Phys. Rev. D **110**, L011901 (2024).
[42] See Supplemental Material at http://link.aps.org/supplemental/10.1103/PhysRevD.110.L111903 for further details on the Heisenberg-Wigner formalism, the field model, further technical information, and additional figures based on these generated data are also displayed, which includes Refs. [43–59].
[43] G. Baym and L. P. Kadanoff, Phys. Rev. **124**, 287 (1961).
[44] L. Keldysh, Zh. Eksp. Teor. Fiz. **47**, 1515 (1964) [, Sov. Phys. JETP **20**, 1018 (1965)], http://www.jetp.ras.ru/cgi-bin/dn/e_020_04_1018.pdf.
[45] E. A. Calzetta and B. L. B. Hu, *Nonequilibrium Quantum Field Theory* (Cambridge University Press, Cambridge, England, 2009), 10.1017/9781009290036.
[46] J. Berges, AIP Conf. Proc. **739**, 3 (2005).
[47] J. Rammer, *Quantum Field Theory of Non-Equilibrium States* (Cambridge University Press, Cambridge, England, 2009).
[48] J. Weinbub and D. K. Ferry, Appl. Phys. Rev. **5**, 041104 (2018).
[49] C. Kohlfürst, arXiv:2212.06057.
[50] C. Kohlfürst, N. Ahmadiniaz, J. Oertel, and R. Schützhold, Phys. Rev. Lett. **129**, 241801 (2022).
[51] F. J. Belinfante, Physica **7**, 449 (1940).
[52] R. Dabrowski and G. V. Dunne, Phys. Rev. D **94**, 065005 (2016).
[53] A. M. Fedotov, E. G. Gelfer, K. Yu. Korolev, and S. A. Smolyansky, Phys. Rev. D **83**, 025011 (2011).
[54] C. K. Dumlu, Phys. Rev. D **79**, 065027 (2009).
[55] V. S. Popov, Zh. Eksp. Teor. Fiz. **62**, 1248 (1972) [Sov. Phys. JETP **35**, 659 (1972)], http://jetp.ras.ru/cgi-bin/dn/e_035_04_0659.pdf.
[56] N. B. Narozhnyi and A. I. Nikishov, Zh. Eksp. Teor. Fiz. **65**, 862 (1973) [Sov. Phys. JETP **38**, 427 (1974)], http://www.jetp.ras.ru/cgi-bin/dn/e_038_03_0427.pdf.
[57] M. Marklund and G. Brodin, Phys. Rev. Lett. **98**, 025001 (2007).
[58] D. Seipt, C. P. Ridgers, D. Del Sorbo, and A. G. R. Thomas, New J. Phys. **23**, 053025 (2021).

[59] C. Kohlfürst, Strong-field quantum electrodynamics in and out-of equilibrium, habilitation thesis, TU Dresden, 2024.
[60] S. P. Gavrilov and D. M. Gitman, Phys. Rev. D **53**, 7162 (1996).
[61] F. Gelis and N. Tanji, Prog. Part. Nucl. Phys. **87**, 1 (2016).
[62] S. Mrowczynski and U. W. Heinz, Ann. Phys. (N.Y.) **229**, 1 (1994).
[63] D. N. Zubarev, Sov. Phys. Usp. **3**, 320 (1960).
[64] P. Zhuang and U. Heinz, Ann. Phys. (N.Y.) **245**, 311 (1996).
[65] D. Vasak, M. Gyulassy, and H. T. Elze, Ann. Phys. (N.Y.) **173**, 462 (1987).
[66] O. T. Serimaa, J. Javanainen, and S. Varró, Phys. Rev. A **33**, 2913 (1986).
[67] I. Bialynicki-Birula, P. Górnicki, and J. Rafelski, Phys. Rev. D **44**, 1825 (1991).
[68] S. Ochs and U. Heinz, Ann. Phys. (N.Y.) **266**, 351 (1998).
[69] P. Zhuang and U. Heinz, Phys. Rev. D **57**, 6525 (1998).
[70] A. Ilderton, Phys. Rev. D **105**, 016021 (2022).
[71] M. Diez, R. Alkofer, and C. Kohlfürst, Phys. Lett. B **844**, 138063 (2023).
[72] C. Gong, Q. Su, and R. Grobe, Phys. Rev. A **109**, 013102 (2024).
[73] C. A. Mancuso, D. D. Hickstein *et al.*, Phys. Rev. A **91**, 031402(R) (2015).
[74] E. Brezin and C. Itzykson, Phys. Rev. D **2**, 1191 (1970).
[75] A. Blinne and H. Gies, Phys. Rev. D **89**, 085001 (2014).
[76] I. Akal, S. Villalba-Chávez, and C. Müller, Phys. Rev. D **90**, 113004 (2014).
[77] A. Otto, D. Seipt, D. Blaschke, B. Kämpfer, and S. A. Smolyansky, Phys. Lett. B **740**, 335 (2015).
[78] E. Strobel and S.-S. Xue, Phys. Rev. D **91**, 045016 (2015).
[79] M. Ruf, G. R. Mocken, C. Müller, K. Z. Hatsagortsyan, and C. H. Keitel, Phys. Rev. Lett. **102**, 080402 (2009).
[80] I. A. Aleksandrov, G. Plunien, and V. M. Shabaev, Phys. Rev. D **94**, 065024 (2016).
[81] Q. Z. Lv, S. Dong, Y. T. Li, Z. M. Sheng, Q. Su, and R. Grobe, Phys. Rev. A **97**, 022515 (2018).
[82] P.-L. He, D. Lao, and F. He, Phys. Rev. Lett. **118**, 163203 (2017).
[83] K. L. Reid, Annu. Rev. Phys. Chem. **54**, 397 (2003).
[84] C. N. Yang, Phys. Rev. **74**, 764 (1948).
[85] M. Ilchen, N. Douguet, T. Mazza *et al.*, Phys. Rev. Lett. **118**, 013002 (2017).
[86] K. Krajewska and J. Z. Kaminski, J. Phys. Conf. Ser. **594**, 012024 (2015).
[87] I. A. Aleksandrov and C. Kohlfürst, Phys. Rev. D **101**, 096009 (2020).
[88] A. I. Nikishov and V. I. Ritus, Zh. Eksp. Teor. Fiz. **52**, 1707 (1967) [Sov. Phys. JETP **25**, 1135 (1967)], http://www.jetp.ras.ru/cgi-bin/dn/e_025_06_1135.pdf.
[89] V. I. Ritus, J. Russ. Laser Res. **6**, 497 (1985).
[90] V. P. Yakovlev, Zh. Eksp. Teor. Fiz. **49**, 318 (1965) [Sov. Phys. JETP **22**, 223 (1966)].
[91] M. H. Mittleman, Phys. Rev. A **35**, 4624 (1987).
[92] F. Karbstein, A. Blinne, H. Gies, and M. Zepf, Phys. Rev. Lett. **123**, 091802 (2019).
[93] Q. Zhao, L. Tang, F. Wan *et al.*, Phys. Rev. D **105**, L071902 (2022).
[94] X. Ribeyre, E. d'Humières, O. Jansen, S. Jequier, V. T. Tikhonchuk, and M. Lobet, Phys. Rev. E **93**, 013201 (2016).
[95] X.-L. Zhu, T.-P. Yu, Z.-M. Sheng, Y. Yin, I. C. E. Turcu, and A. Pukhov, Nat. Commun. **7**, 13686 (2016).
[96] A. Mercuri-Baron, M. Grech, F. Niel, A. Grassi, M. Lobet, A. Di Piazza, and C. Riconda, New J. Phys. **23**, 085006 (2021).
[97] T. G. Blackburn and B. King, Eur. Phys. J. C **82**, 44 (2022).
[98] N. Mahlin, S. Villalba-Chávez, and C. Müller, Phys. Rev. D **108**, 096023 (2023).
[99] B. Kettle, D. Hollatz, E. Gerstmayr, G. M. Samarin, A. Alejo, S. Astbury, C. Baird, S. Bohlen, M. Campbell, C. Colgan *et al.*, New J. Phys. **23**, 115006 (2021).
[100] F. C. Salgado, K. Grafenstein, A. Golub, A. Döpp, A. Eckey, D. Hollatz, C. Müller, A. Seidel, D. Seipt, S. Karsch *et al.*, New J. Phys. **23**, 105002 (2021).
[101] C. Kohlfürst, version 1, RODARE, 10.14278/rodare.3337 (2024).